Divergent processing of FVIII light chain variants: secretory potential *versus* proteasomal retention

Heike Singer,[1*] Payal Chawla,[1*] Katrin J. Czogalla-Nitsche,[1] Pujan Engels,[1] Francesco Forin,[1] Marc Sylvester,[2] Melanie Rath,[1] Jens Müller,[1] Tobias Feist,[1] Behnaz Pezeshkpoor,[1] Rawya Al-Rifai,[1] Osman El-Maarri[1] and Johannes Oldenburg[1]

[1]Institute of Experimental Haematology and Transfusion Medicine and [2]Medical Faculty, Core Facility Mass Spectrometry, Institute of Biochemistry and Molecular Biology, University of Bonn, Bonn, Germany

**HS and PC contributed equally as first authors.*

Correspondence: J. Oldenburg
johannes.oldenburg@ukbonn.de

Received: May 15, 2025.
Accepted: November 14, 2025.
Early view: November 27, 2025.

https://doi.org/10.3324/haematol.2025.288250

Abstract

In 20-30% of severe hemophilia A (HA) patients, FVIII replacement therapy is hindered by inhibitory antibodies. Nonsense mutations in the FVIII light chain (A3-C1-C2) carry a higher risk of inhibitor formation than those in the heavy chain (A1-A2-B). The underlying molecular mechanism remains unclear. Using induced pluripotent stem (iPS) cells from HA patients, we developed two types of endothelial cell models, induced lymphatic endothelial cells (iLEC) and induced liver sinusoidal endothelial cells (iLSEC), that mimic native *F8* mRNA expression and protein synthesis. Immunoassays detected FVIII protein in wild-type, intron 22 inversions (I22I), and two high inhibitor risk light chain variants (R1960X, R2228X). Co-staining with ER markers (PDI, BiP) revealed differential processing: R1960X exhibit enhanced proteasomal degradation with SEL1L, essential for MHC-I peptide loading, possibly contributing to higher immunogenicity. In contrast, R2228X showed a pattern more similar to wild-type, suggesting partial secretory potential. Although a mild co-localization with SEL1L was observed, it was not significant. Clinically, this patient did not develop inhibitors. In addition, exploratory *in silico* peptide binding predictions suggested that R1960X may generate a higher number of FVIII-derived epitopes presented via patient-specific HLA alleles compared to R2228X, further supporting differential immunogenicity. The I22I variant also showed detectable FVIII protein, which was deglycosylated and retained in the ER but did not co-localize with SEL1L; no inhibitor was observed in this case either. This cellular model shows reduced variability compared to primary cells, enabling patient-specific FVIII variant analyses, including intracellular processing, within the genetic background of the individual patient.

Introduction

Hemophilia A (HA) is an X-linked disorder resulting from mutations in the *F8* gene, encoding the coagulation factor VIII (FVIII).[1] HA patients can be treated by the administration of exogenous FVIII. However, the therapy can lead to the development of anti-drug antibodies (ADA) in approximately 30% of severe HA patients, directed against the A2, A3, C1, or C2 domains of the FVIII molecule.[2] These inhibitors are produced in a $CD4^+$ T-cell dependent manner, when foreign FVIII peptides are presented on the MHC class II molecules.[3] Additionally, single nucleotide polymorphisms in immune-specific genes such as *TNF*-α, *IL10* and *CTLA-4* play a role in the patient immunogenicity.[4-6]

The *F8* genotype plays a crucial role in inhibitor formation. Among null mutations, large deletions are associated with the highest risk, followed by nonsense mutations and intron 22 inversions (I22I), which result in a complete absence of FVIII protein synthesis.[3] However, the risk of inhibitor development also depends on the type of mutation and their location with the light chain domains being more immunogenic than those located in the heavy chain domains.[3,7,8] Additionally, *F8* stop mutations in the B domain demonstrated basal readthrough beyond the premature termination codons (PTC), resulting in the synthesis of residual FVIII antigen measured from patient plasma suggesting the presence of non-functional or partially functional protein.[9] Residual truncated FVIII protein in I22I patients has been previously detected, by immunohistochemical staining of human I22I liver explant. The missing protein part may be compensated by F8B, which could explain the lower risk of inhibitor development.[10] Nevertheless, due to the lack of antibody specificity, the actual FVIII expression in I22I can still not be determined.[11]

Despite these insights, the mutation-specific molecular mechanisms leading to the higher risk of inhibitors re-

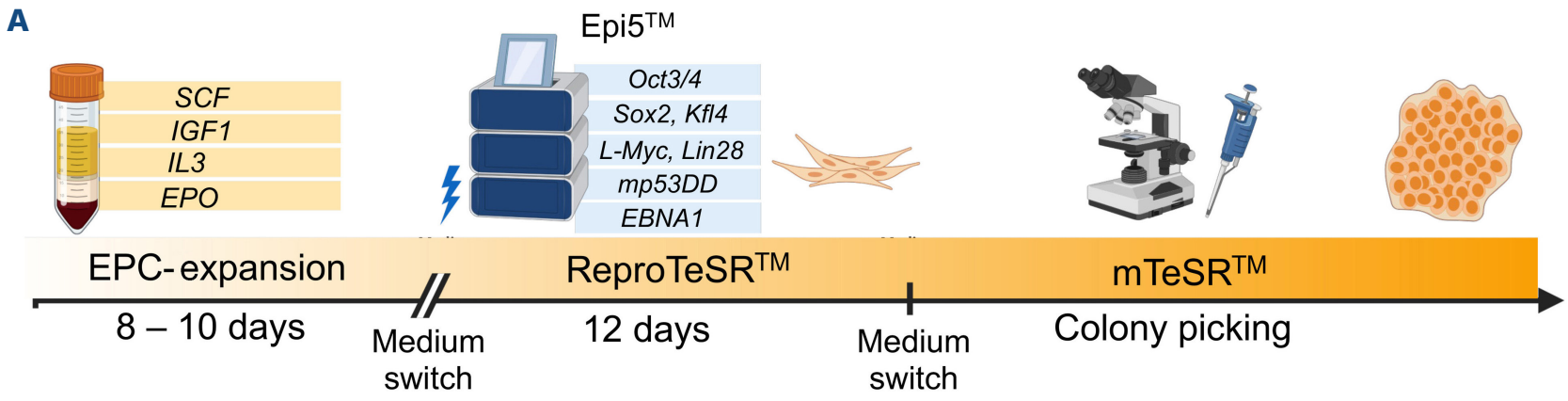

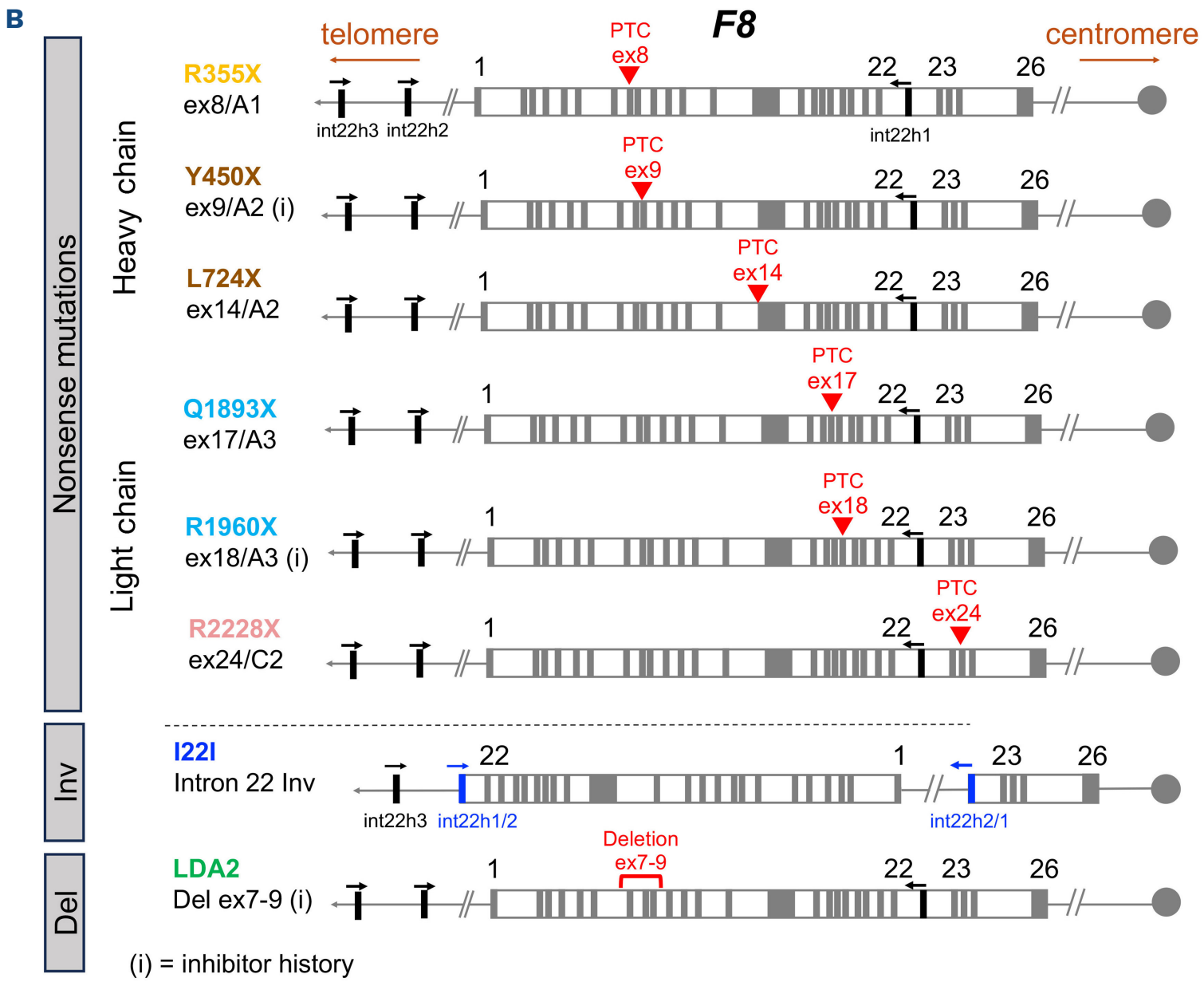

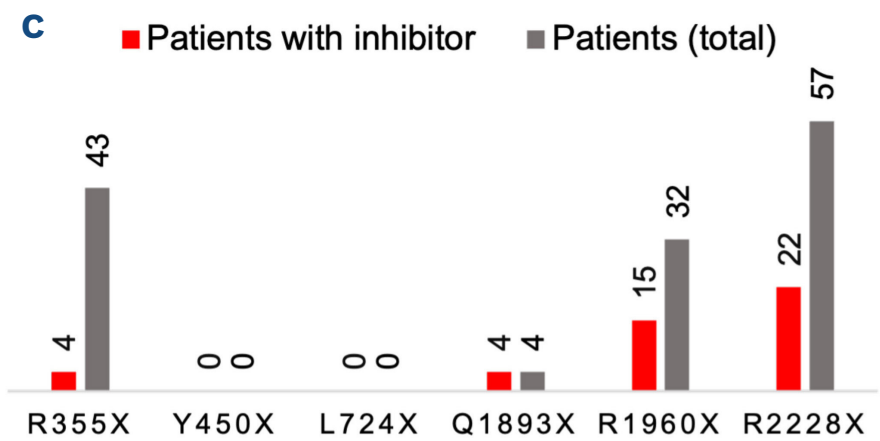

Figure 1. Reprogramming timeline and overview of hemophilia A patient samples. (A) Schematic overview of the reprogramming workflow. Patient-derived peripheral blood mononuclear cells were expanded in StemSpan™ medium for 8-10 days before electroporation with Epi5™ episomal vectors containing reprogramming factors. Following reprogramming, cells were cultured in ReproTeSR™ medium for 12 days before colonies were picked for clonal expansion (mTeSR™) and quality control. Induced plurip-

Continued on following page.

otent stem cell lines were generated from one healthy male control and 8 patients with severe hemophilia A. (B) Overview of patient-specific FVIII mutations. The panel shows schematic representations of the *F8* gene with the positions of nonsense mutations (PTC), an intron-22 inversion (I22I), and a large deletion (LDA2). Mutations are grouped by location in the heavy chain (top) or light chain (bottom). Mutations associated with a history of inhibitor development are indicated with (i). Red triangles represent PTC positions within corresponding exon. (C) Reported cases of HA patients with nonsense mutation (gray) and their associated inhibitor incidences (red) demonstrating that PTC located in the region coding for FVIII light chain (aa1648-2332) have a higher risk for FVIII inhibitors than PTC located in regions coding for the heavy chain (aa1-aa741). Data generated by FVIII mutation data base; www.factorVIII-db.org.

main poorly understood. While the synthesis of a residual full-length FVIII could lower inhibitor development, the endogenous levels of a truncated protein may alter central or peripheral tolerance, causing immunogenicity.[12]

The FVIII protein is synthesized in endothelial cells (EC), such as liver sinusoidal endothelial cells (LSEC), microvascular endothelial cells (MVEC), and lymphatic endothelial cells (LEC).[13-15] However, primary EC exhibit intrinsic heterogeneity in terms of their proliferation potential, marker expression, and functionality.[16] This variability can complicate disease modeling and therapeutic studies. Differentiation of induced pluripotent stem (iPS) cells into more homogenous EC subtypes provides a robust platform to study the synthesis of FVIII.[17,18] Additionally, patient iPS cell-derived EC models enable analysis of *F8* mutations on FVIII protein expression and translation reflecting individual genetic variation.

Induced pluripotent stem cells were generated from peripheral blood mononuclear cells (PBMC) of 6 HA patients with nonsense mutations, one patient with I22I and one with a large deletion in the A2 domain (Figure 1A). The location of the respective mutations within the *F8* gene is illustrated in Figure 1B. Inhibitor history of the reported mutations is summarized in Figure 1C. The patient-specific iPS cells were differentiated into iLEC and iLSEC to study endogenous *F8* expression on the mRNA and protein levels. The established cellular model contains all exon-intron boundary junctions capable of reflecting the endogenous mutational framework.

We identified FVIII variants within patient-derived iLEC and iLSEC with nonsense mutations R1960X and R2228X in the light chain and confirmed the existence of an I22I variant in our cellular models. Furthermore, the FVIII nonsense variants were found to co-localize with SEL1L (Suppressor / Enhancer of Lin-12-like), a known facilitator of proteasomal degradation. These results provide interesting insights into the cellular processing of FVIII variants and could help tackle immunogenicity challenges in HA replacement therapy.

Methods

Blood samples and reprogramming

Blood samples were collected from 8 severe HA patients and a healthy male control (Cm1). Samples were obtained after written informed consent. The local ethics committee of the University Clinic of Bonn approved the study (number 244/19). PBMC were isolated and reprogrammed as per the previously published protocol.[19]

Differentiation of induced pluripotent stem cells into induced lymphatic endothelial cells and induced liver sinusoidal endothelial cells

2D monolayer differentiation from iPS cells into vascular EC (vEC) was performed according to a published protocol.[20] These cells were further used for downstream applications (see *Online Supplementary Methods*). bFGF and L-685-458 were only added when differentiating into iLSEC. Day 6 angioblasts for both subtypes were seeded at a cell density of $5.2x10^4$ cells/cm^2 on tissue culture plates coated with fibronectin.

Differentiation into iLEC - $CD144^+$ angioblasts were maintained in ECGM-MV2 medium supplemented with VEGF-A.

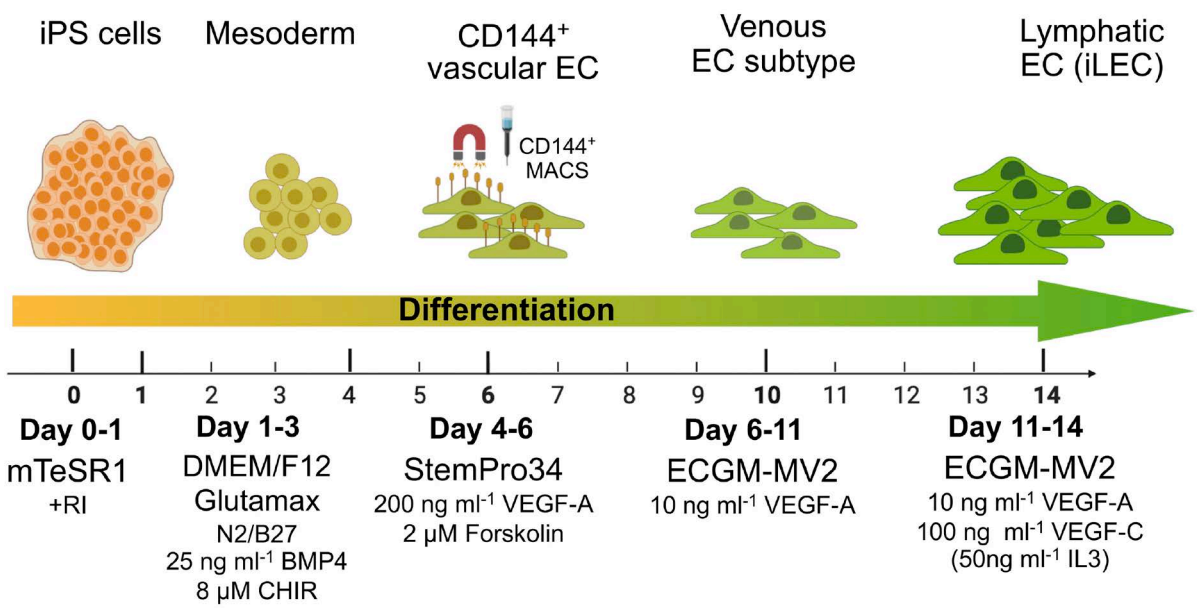

Figure 2. Differentiation of induced pluripotent stem cells into vascular and lymphatic endothelial cell models. Induced pluripotent stem (iPS) cells were directed into mesodermal lineage using CHIR and BMP4. After a medium switch on day 4, cells were differentiated into vascular endothelial cells. Cells were either maintained in the presence of low VEGF-A or combined with 100 ng VEGF-C and 50 ng IL3 to achieve induced lymphatic endothelial cell (iLEC) fate.

Starting day 11 until day 14, VEGF-C and IL3 were added (Figures 2, 3).

Differentiation into iLSEC - CD34+ angioblasts were maintained under hypoxic conditions (37°C, 5% CO_2, 5% O_2, 95% N_2). Cell medium was a combination of StemPro™-34 and ECGM-MV2 (1:1) supplemented with VEGF-A and bFGF (E/S) or complete ECGM-MV2 medium supplemented with VEGF-A (E). On day 10, LSEC induction (LI) medium was supplemented with SB-431542, 8-Br-cAMP +/- bFGF. Medium was replaced every second day until day 16 (Figures 4, 5). Characterization and functional assays were conducted.

ELISA

Day 14 iLEC and iLSEC were harvested, counted, and resuspended in NP-40 lysis buffer containing protease inhibitor. Cells were adjusted to a concentration of $1x10^6$ cells per 50 µL lysis buffer, and the corresponding volume of buffer was added to the cell pellet. Using our in-house established ELISA, lysates were applied at a 1:6 dilution in triplicates, corresponding to approximately $1.7x10^5$ cells per well. GMA012 (anti-A2) or CaptureSelect™ biotin anti-FVIII conjugate (anti-A3) were used as capture antibodies. SAF8C-HRP was used for detection by luminescence

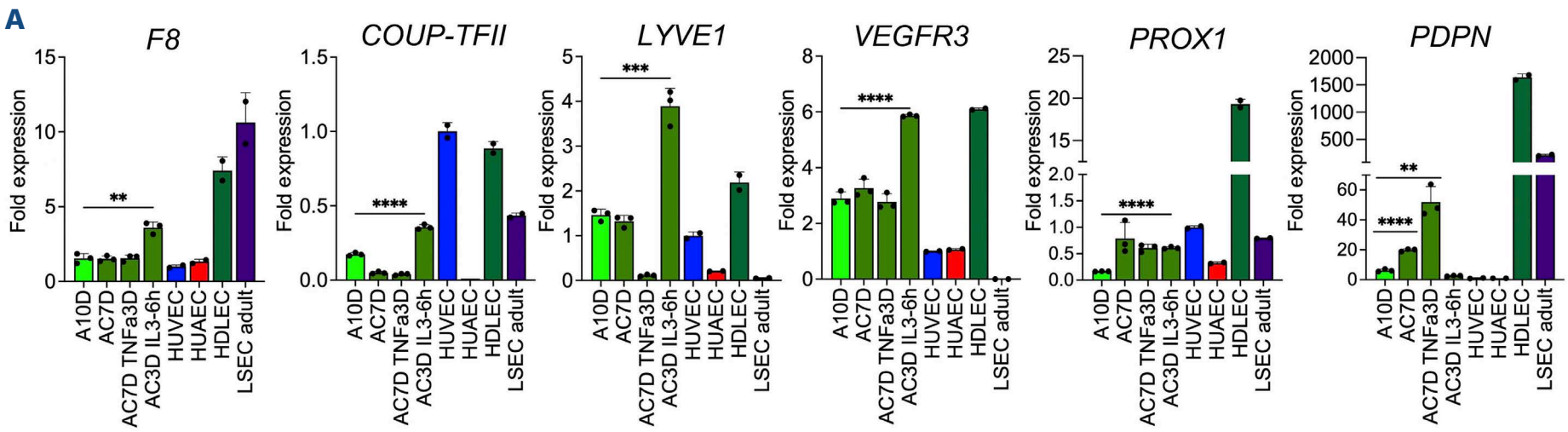

Figure 3. Specification analysis of induced pluripotent stem cell-derived vascular and lymphatic endothelial cell models. (A) RT-PCR analysis of cell-specific markers in vascular endothelial cell (A10D) and induced lymphatic endothelial cell (iLEC) using F8, COUP-TFII, LYVE1, VEGFR-3, PROX1 and PDPN. Maintenance of cells in ECGM-MV2 after CD144 MACS isolation on day 6. A10D: adding ten days VEGF-A (day 6-16); AC7D: adding seven days VEGF-A and VEGF-C (day 6-13); AC7D TNF-α: adding seven days VEGF-A and VEGF-C (day 6-13) with three days cytokine stimulation using TNF-α (day 10-13); AC3D IL3-6h: adding five days VEGF-A (day 6-11), adding three days VEGF-C and VEGF-A (day 11-14), on day 14 cytokine stimulation for 6 hours with IL3; pHUVEC: human umbilical vein endothelial cell; pHUAEC: human umbilical arterial endothelial cell; pHDLEC: human dermal lymphatic endothelial cell; pLSEC: liver sinusoidal endothelial cell. N=200,000 cells. Unpaired *t* test: **P*<0.05, ***P*<0.01, ****P*<0.001, *****P*<0.0001. Results demonstrated as a fold change to pHUVEC. (B) Flow cytometry analysis of CD144 and VEGFR3 surface expression in vEC and iLEC. N=500,000 cells. Expression as percentage of positive populations. (C) Immunostaining of iLEC (AC3D IL3-6h) differentiated cells. Lymphatic marker PROX1 (green) and LYVE1 (red). Venous marker COUP-TFII (green). General EC Marker CD31 (red), CD144 (green), and von Willebrand factor (VWF) (red). Nuclei were counterstained in DAPi. Images were acquired using an Axio Observer 7 microscope with ApoTome.2. The objective used was a Plan-Apochromat 20x/0,8 M27. Images were captured with an AxioCam 702 Mono camera. Results shown as a representative image of biological triplicates.

read-out. Quantification was based on a standard curve prepared using HEK *F8*$^{-/-}$ lysate (1:6, as for the samples) combined with recombinant full-length FVIII (Kogenate) (5, 7.5, 10, 20, 40, 80, 160, 320 mU/mL).

Western blot

Lysate of 1x10^{7} differentiated iLSEC was prepared using NP-40 lysis buffer and purified using 50 kD-MW cut-off Vivaspin columns. The purified lysate was incubated with SAF8C-AP or GMA012 for one hour, followed by purification using the CaptureM™ IP and Co-IP kit. Eluted proteins were loaded on 7.5% TGX gel. Western blot was conducted using GMA012 or SAF8C-AP antibody with an overnight incubation at 4°C.

Sample digestion for mass spectrometry

Purified cell eluents (as used for western blot) were subjected to cysteine reduction and alkylation with 20 mM DTT and 40 mM acrylamide in 50 mM triethylammonium bicarbonate (TEAB). A mixture of hydrophilic carboxylate-coated magnetic beads was employed. FVIII protein binding was induced with ethanol. After a brief washing step with ethanol, the bound peptides were subjected to overnight tryptic digestion at 37°C. Peptide solutions were separated from the magnetic beads, dried, and further desalted with C18 ZipTips. (See *Online Supplementary Methods*).

Further information on the methods and reagents used in the study is provided in the *Online Supplementary Methods* and in *Online Supplementary Table S1*.

Results

Generation of induced pluripotent stem cells cells from HA patient-derived peripheral blood mononuclear cells

Peripheral blood mononuclear cells were isolated from blood and expanded for erythroid progenitor cells. After episomal reprogramming, iPS cell clones appeared between days 9 and 12 (Figure 1A). We confirmed pluripotency by APLive- and subsequent immunostaining of the stem cell markers Nanog, SSEA-4, Tra-1-60 and Oct4. Ability to differentiate into all three germ layers was confirmed *in vitro* for each clone (*Online Supplementary Figures S1, S2*). Silencing of the transgene was validated by endpoint PCR, proving the absence of episomal vectors in each iPS cell clone (*Online Supplementary Figure S1*). Genomic integrity was confirmed by SNP-array (*Online Supplementary Figure S3*). CRISPR/Cas9 knockout of *F8* (F8$^{-/-}$) was generated from the Cm1 IPS clone (*Online Supplementary Figure S4*).

Enhancing FVIII synthesis in induced pluripotent stem cell-derived endothelial cells to improve FVIII detection

Induced pluripotent stem cells were differentiated towards the mesodermal lineage (Figure 2) utilizing BMP4 and CHIR, a small molecule inhibitor of WNT signaling. Mesoderm was induced towards a vascular endothelial lineage by introducing high concentrations of VEGF-A (200 ng) and forskolin (*Online Supplementary Figure S5*). On day 6, CD144^{+} EC were cultured with VEGF-A (10 ng), to direct the cells into a venous lineage. These models were consistently compared with primary (p) EC, including pHUVEC, pHDLEC and pLSEC. pHDLEC exhibited high *F8* expression, comparable to pLSEC. The lymphatic endothelial cell markers *LYVE1, VEGFR-3, PROX1* and *PDPN* (*Podoplanin*) were highly expressed in pHDLEC, differing significantly from the pLSEC profile (Figure 3A and *Online Supplementary Figure S6*).

Induced pluripotent stem cell-derived vEC established a venous identity with no significant difference in *F8* expression (Figure 3A, A10D, and *Online Supplementary Figure S7A*). Treatment with VEGF-C +/- angiopoietin for three additional days directing vEC towards lymphatic cells resulted in an increase in the expression levels of *LYVE1* and *VEGFR-3*. No or low expression of *PROX1, PDPN* and *F8* was

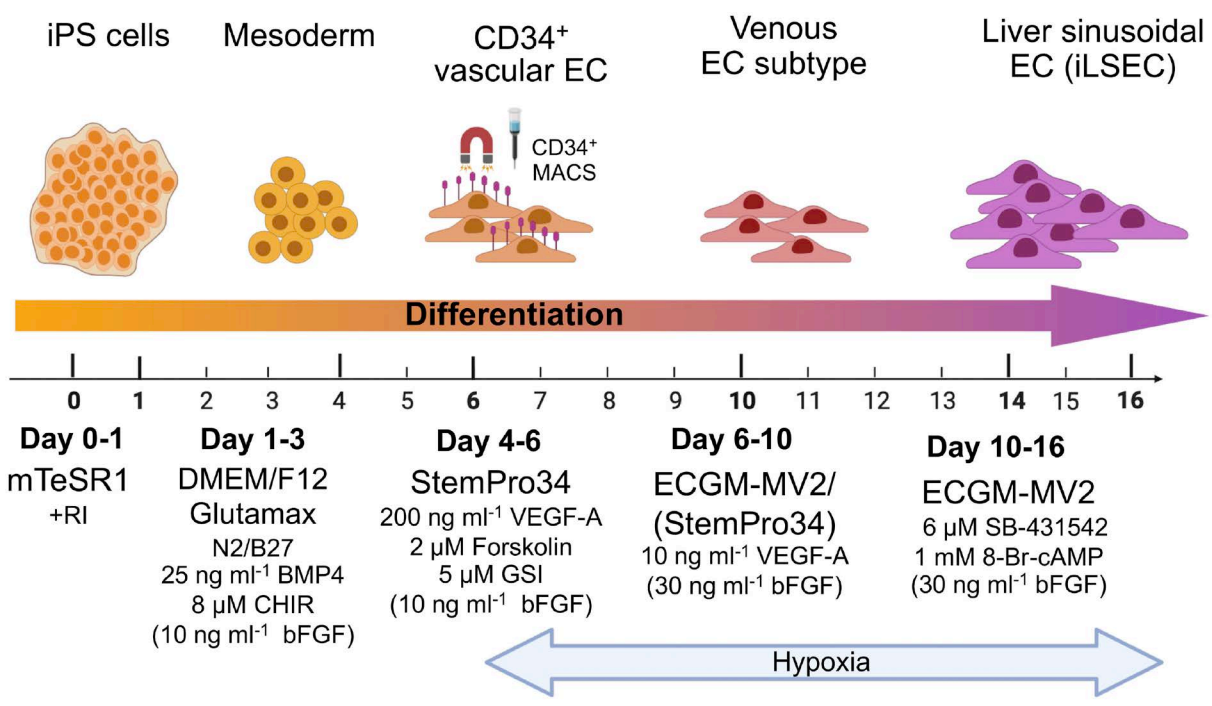

Figure 4. Differentiation of induced pluripotent stem cells into liver sinusoidal endothelial cell model. Timeline for differentiation of induced pluripotent stem cells into liver sinusoidal endothelial cell model (iLSEC) was identical to vascular endothelial cells (vEC) until day 6 except the presence of gamma-secretase inhibitors (GSI) for directed differentiation towards the venous lineage (day 4-6). CD34^{+} cells were MACS isolated. Cells were further maintained for four days in low VEGF-A conditions and induced for the LSEC fate. Starting day 10, LSEC induction (LI) started, and cells were maintained in hypoxia.

observed (T1, T2) (*Online Supplementary Figure S7B, C*). Inflammatory cytokine IL3 resulted in a 2-fold increase in *F8* expression and upregulation of *COUP-TFII, LYVE-1, VEGFR-3* and *PROX1*, without notable changes in *PDPN* (Figure 3A, AC3D-IL3-6h, and *Online Supplementary Figure S8*). FACS confirmed VEGFR-3 expression in populations treated with both VEGF-C and IL3. CD144 expression was stable under both conditions (Figure 3B). Immunofluorescence (IF) confirmed LEC marker expression of PROX1, COUP-TFII, LYVE1, CD31, CD144 and VWF when treated with a combination of VEGF-A, VEGF-C and IL3 (AC3D IL3-6h, Figure 3C). VEGF-A and VEGF-C treatments over seven days (Figure 3A, AC7D), or in combination with TNFα on days 11-13 (Figure 3A, AC7D TNFα 3D), demonstrated no significant changes in *F8*. However, addition of TNFα significantly increased *COUP-TFII* and *PDPN* levels (Figure 3A, AC7D TNFα 3D).

Since LSEC are a known primary site for FVIII synthesis,[21] we differentiated iPS cells into LSEC to study the expression of *F8*. We adapted a previously published protocol[17] implementing key modifications (Figure 4). Mesoderm was induced under normoxia. $CD34^+$ MACS selected angioblasts were subjected to hypoxia and maintained until day 10. Two medium conditions to induce a venous subtype were evaluated (see Methods). For LSEC induction, both media conditions implemented 8-Br-cAMP and TGFβ inhibitor SB-431542 fostering the expression of LSEC markers STAB2, LYVE1 and *FCGR2b*.[17,22] Arterial, venous and LSEC-specific markers were analyzed by RT-PCR, FACS and IF staining (Figure 5A-C). From lineage tracing studies, it has been established that a venous positive population leads to the development of LSEC specification.[23,24] The $CD34^+$ population was confirmed in both treatment conditions (Figure 5B, *Online Supplementary Figure S9*). VEGF-A down-regulates notch signaling, promoting venous specification with 86.7% $CD73^+$ population (LI-4D E/S) and 74.2% for LI-6D E. Both conditions show a $CD184^{low}$ population due to the combined effect of gamma-secretase inhibitors (GSI) and notch signaling inhibition. LI-2D E/S demonstrated a 3.3-fold increase in *F8* compared to A10D while longer treatment observed lower expression values (LI-4D E/S) similar to LI-6D E. LI-2D E/S additionally exhibited a significant increase in *COUP-TFII, STAB2* and *FCGR2b* expression, while *FCGR2b* maintained a stable expression across all three conditions. *VEGFR3* showed a slight significant increase in LI-2D E/S and LI-4D E/S samples. *PROX1* and *PDPN* expression levels were elevated in all three conditions compared to A10D. *LYVE1* expression was up-regulated only under E/S conditions (Figure 5A). IF confirmed the expression of PROX1, COUP-TFII, CD31, LYVE1, STAB2 and VWF in iLSEC (LI-4D E/S, Figure 5C). Treatment with IFNγ confirmed inflammatory responsiveness and increased *CIITA* expression and consequently enhanced MHC-II levels in iLSEC, but also in vEC (A10D) (*Online Supplementary Figure S10*).

Transcript integrity, synthesis and detection of the FVIII protein

We detected full-length *F8 mRNA* in iPS cell-derived vEC from all 6 patient samples containing premature termination codons (PTC), indicating presence of normal splicing product when compared to Cm1 (*Online Supplementary Figure S11*). The analysis of *F8 mRNA* in patient sample I22I revealed the expected break between exons 22 and 23 due to the lack of amplification of region D. Nested PCR designed to span exons 19-24 and 24-26 failed to produce any amplifiable products. Exons 1-8 of rendered region A were not amplified for the patient sample LDA2 (exons 7-9). This absence of PCR products extended to nested regions exons 1-5 and 4-8. No amplification was observed between exons 8 to 11.

To confirm the synthesis of FVIII, we utilized a robust mass spectrometry-based method for detecting and quantifying proteins. Six unique endogenous peptides from Cm1, with a false discovery rate (FDR) of 1% (Figure 6A and *Online Supplementary Table S2*) were detected. Peptides were identified from multiple domains within the FVIII protein: DFPILPGEIFK and NVILFSVFDENR derived from A2, GELNEHLGLLGYPIR from A3, VDLLAPMIIHGIK from C1, and the peptides SNAWRPQVNNPK and IHPQWVHQIALR from the C2 domain across three separate measurements. These results indicate the integrity and completeness of the synthesized protein. IF was conducted to detect and visualize the low abundant FVIII. Biotin anti-FVIII conjugate was determined to be effective after rigorous evaluation and comparison with various FVIII-specific monoclonal antibodies used for IF and ELISA results (*data not shown*). FVIII was detected in pLSEC and iLSEC, confirming endogenous FVIII synthesis. No signal was detected in the Cm1 $F8^{-/-}$ (Figure 6B).

ELISA measurements were also performed on lysates from iLEC of Cm1, I22I, LDA2 and six nonsense mutations. GMA012 detected FVIII-Ag for both Cm1 and I22I samples, which served as positive controls (Figure 7A). FVIII-Ag was also detected for R1960X and R2228X, when normalized against LDA2 (negative control). Additionally, iLSEC lysates from Cm1, I22I, Cm1 $F8^{-/-}$, LDA2 and nonsense mutations, were analyzed, and detected FVIII-Ag in Cm1, I22I, and R1960X and R2228X. Biotin anti-FVIII conjugate confirmed the presence of FVIII in Cm1, while the Cm1 $F8^{-/-}$ and LDA2 samples remained negative. FVIII-Ag was also observed for R1960X and R2228X, albeit at different levels.

Molecular characterization of FVIII variants and intracellular processing

To investigate the intracellular expression and processing of FVIII variants, we first performed immunoprecipitation using the polyclonal anti-FVIII antibody SAF8C-AP, followed by western blot detection with the monoclonal anti-A2 antibody GMA012 (Figure 7B). In Cm1, a strong 250 kDa band and 100-200 kDa smear was observed representing the

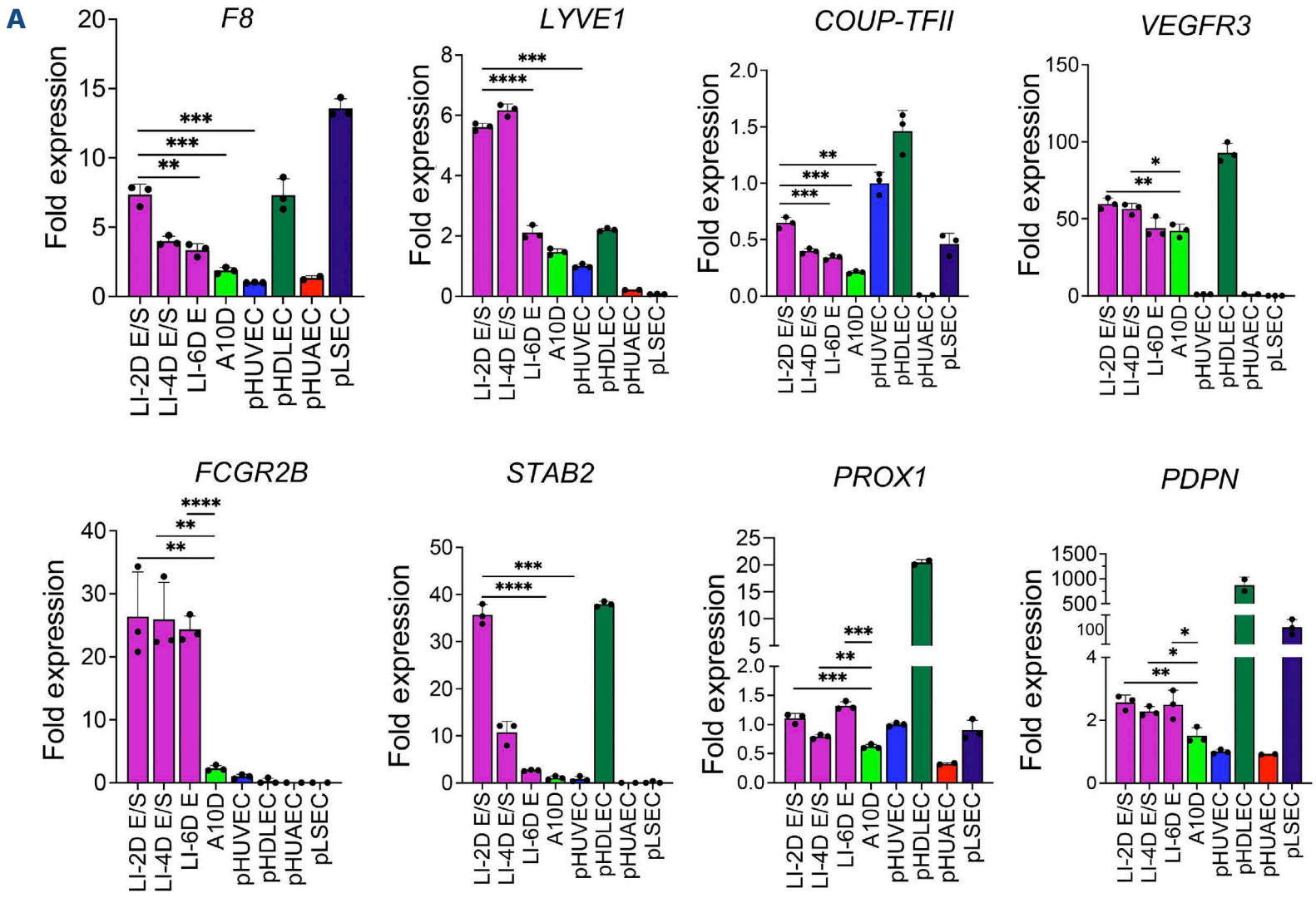

Continued on following page.

Figure 5. Specification analysis of induced pluripotent stem cell-derived liver sinusoidal endothelial cell models. (A) RT-PCR analysis of cell specific markers in vascular endothelial cells (A10D) and liver sinusoidal endothelial cells (iLSEC) using *F8, COUP-TFII, FCGR2b, Stab2, LYVE1, VEGFR-3, PROX1* and *PDPN*. LI-2D E/S: two days LI; 1:1 ECGM-MV2 and StemPro-34; LI-4D E/S: four days LI; 1:1 ECGM-MV2 and StemPro-34; LI-6D E: six days LI, only ECGM-MV2. E/S medium conditions consist of bFGF. Cells cultured in medium condition E does not contain bFGF. A10D: from generic vEC protocol, adding ten days VEGF-A (Day 6-10). pHUVEC: human umbilical vein endothelial cell; HUAEC: human umbilical arterial endothelial cell; pHDLEC: human dermal lymphatic endothelial cell; pLSEC: liver sinusoidal endothelial cell. N=200,000 cells. Unpaired *t* test significance: **P*<0.05, ***P*<0.01, ****P*<0.001, *****P*<0.0001. All data points indicate mechanical duplicates. Results demonstrated as a fold change to pHUVEC. (B) Flow cytometry analysis of endothelial surface markers KDR and CD34, and of venous and arterial $CD34^{+}$ subpopulations defined by venous marker CD73 (purple), arterial marker CD184 (pink) and dual positive (black) cells in iLSEC. N=500,000 cells. Data shown as percentage of positive populations. (C) Immunostaining results of LI-6D E treated cells for PROX1 (green), COUP-TFII, CD31, LYVE1, STAB2, and VWF (all red). Nuclei were counterstained with DAPi. Images were acquired using an Axio Observer 7 microscope with ApoTome.2. The objective used was a Plan-Apochromat 20x/0,8 M27. Images were captured with an AxioCam 702 Mono camera. Results depicted as a representative image of biological triplicates.

full-length single-chain FVIII and furin cleaved heavy chain products, respectively. I22I showed a distinct single-chain product between 240-250 kDa and faint bands around the 160-170 kDa and 110-150 kDa range, suggesting altered processing compared to Cm1. A faint band was observed for R2228X around 240 kDa and 100-130 kDa, suggestive of targeted degradation. R1960X exhibited an extensive smear between 80-230 kDa and a faint signal around 240 kDa, indicating degradation and incomplete processing.

To assess glycosylation and processing, immunoprecipitation using GMA012, detection with SAF8C-AP before and after PNGase F treatment was conducted (Figure 7C). In Cm1, deglycosylation converted the heavy chain bands at 120-200 kDa (Figure 7C, left panel) into a sharp band at 160-170 kDa (HC). In addition, glycosylated single-chain product SC^{Glyc} (>260 kDa) shifted to approximately 250 kDa (SC) following PNGase F treatment (Figure 7C, right panel), confirming N-linked glycosylation and processing. I22I displayed two stable bands at approximately 250 kDa (SC^{mut}) and 160-170 kDa (HC) both before and after PNGase F treatment, without mobility shift, indicating a lack of glycosylation and accumulation of a truncated proteolytic FVIII product in the ER. R2228X variant showed a similar glycosylation-dependent shift of the heavy chain upon treatment as observed in Cm1, while the single chain product (SC^{mut}) remained unchanged. In contrast, R1960X displayed faint SC^{mut} and HC signals with a broad smear that intensified after PNGase F treatment, indicative of instability, misfolding, and impaired deglycosylation, resulting in accumulation of degraded intermediates.

Notably, the banding patterns differ between SAF8C (polyclonal) and GMA012 (monoclonal A2) immunoprecipitation. For I22I, both the 240-250 kDa SC^{mut} and 160-170 kDa HC species are consistently detectable with both antibodies, although SAF8C enriches a stronger single chain product and an additional 100-150 kDa product that is not recovered with GMA012, most likely due to the lack of an accessible A2 epitope. For R1960X, SAF8C IP reveals a broad smear of heterogeneous degradation products, whereas GMA012 selectively precipitates only weak A2-containing species with residual signals around 160-170 kDa, indicative of degraded heavy chain-related intermediates.

A

Sample	Peptides found	Domain	Positions
Cm1	DFPILPGEIFK	A2	519-529
	NVILFSVFDENR	A2	591-602
	GELNEHLGLLGPYIR	A3	1769-1783
	VDLLAPMIIHGIK	C1	2092-2104
	SNAWRPQVNNPK	C2	2235-2246
	IHPQSWVHQIALR	C2	2327-2339

B

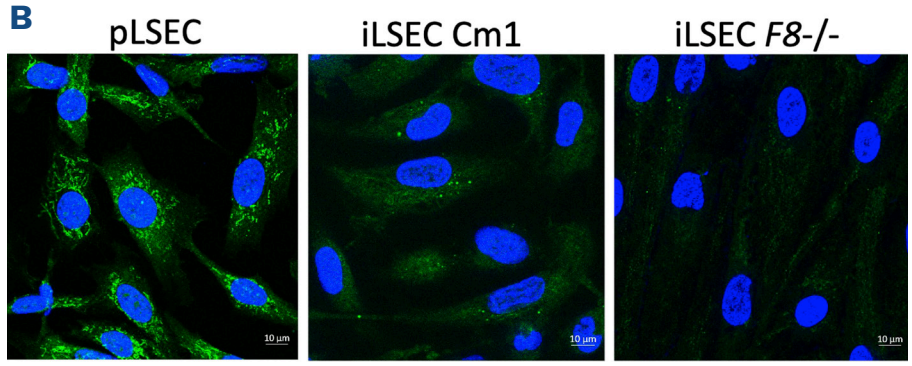

Figure 6. Detection of endogenous FVIII protein in wild-type induced liver sinusoidal endothelial cells by liquid chromatography / mass spectrometry and immunofluorescence. (A) List of targeted liquid chromatography/mass spectrometry (MS) measurements of endogenous FVIII peptides identified by MS (N=6). Biological duplicates of healthy donor. (B) Immunostaining with biotin anti-FVIII conjugate targeting the A3 domain of FVIII visualized with Streptavidin488 (green) in primary liver sinusoidal endothelial cells (pLSEC) and induced pluripotent stem cell-derived LSEC (iLSEC). iLSEC Cm1: wild-type, iLSEC $F8^{-/-}$: F8 knockout. Nuclei were counterstained with DAPi. Images were acquired using an Axio Observer 7 microscope with ApoTome.2. The objective used was a Plan-Apochromat 40x/1.4 Oil DIC M27. Images were captured with an AxioCam 702 Mono camera. Results depicted as a representative image of biological triplicates.

FVIII and von Willebrand factor follow distinct trafficking routes in induced and primary endothelial cells

Protein disulfide isomerase (PDI), an endoplasmic reticulum (ER) marker, and COPII as a marker for the ER-Golgi intermediate compartment (ERGIC) were used to localize FVIII in iLSEC (Figure 8A). FVIII accumulated within the ER with minimal co-localization with COPII, indicating limited

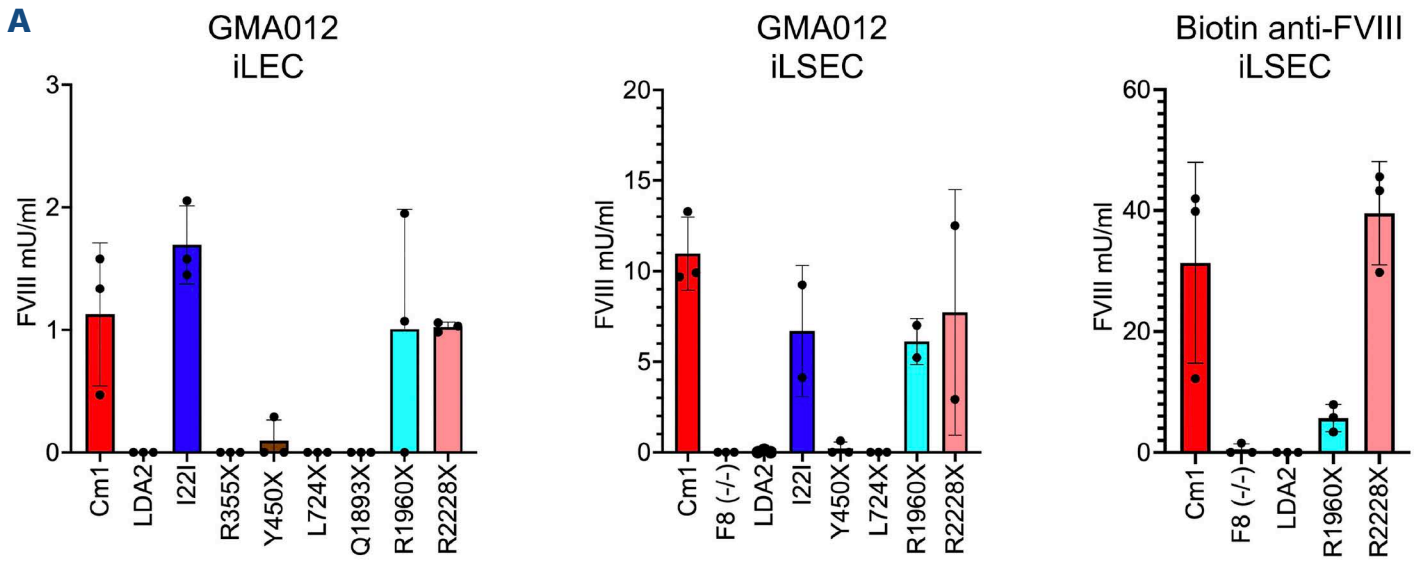

Figure 7. Intracellular detection of FVIII protein variants and N-glycosylation status in induced pluripotent stem cell-derived endothelial cells. (A) ELISA quantification of FVIII antigen in induced liver endothelial cells (iLEC) and in induced liver sinusoidal endothelial cells (iLSEC) using anti-FVIII-A2 (GMA012) and anti-FVIII-A3 (biotin anti-FVIII conjugate). Results show detectable FVIII antigen in wild-type (Cm1) and selected mutant variants (I22I, R1960X, R2228X), with lower levels in F8 ($^{-/-}$) or LDA2 negative controls, confirming intracellular FVIII expression in induced pluripotent stem cell-derived endothelial cells. (B) Western blot analysis of immunoprecipitated FVIII protein using SAF8C-AP (IP) and GMA012 (WB). Cell lysates (1x10^7 cells/sample) from wild-type control (Cm1), I22I, R2228X, R1960X and F8KO were analyzed. Molecular weight marker is shown on the left. Results are representative of biological duplicates. The full-length wild-type single-chain FVIII (~250 kDa) is marked with a red asterisk, and the furin-cleaved heavy chain (100-200 kDa) with a red bracket. The blue asterisk indicates the I22I single-chain product (240 - 250 kDa); the blue triangle (160-170 kDa) and blue bracket (110-150 kDa) mark additional faint bands. The R2228X single-chain product (~240 kDa) is marked with a pale-pink asterisk, and the pale-pink bracket highlights a faint band between 100 and 130 kDa. The R1960X single-chain product (~240 kDa) is indicated by a cyan asterisk, while the cyan bracket marks the broad smear between 80-230 kDa. The FVIII-knockout control (F8KO) showed no signal. (C) Western blot analysis of immunoprecipitated FVIII protein using GMA012 (IP) and SAF8C-AP (WB) before and after PNGase F treatment. Cell lysates (1x10^7 cells/sample) from wild-type control (Cm1), intron 22 inversions (I22I), R2228X and R1960X were analyzed. Molecular weight marker is shown on the left. Results are representative of one single experiment. In Cm1, the glycosylated single-chain FVIII (SC^{Glyc}, >260 kDa) and heavy-chain species (HC, 120-200 kDa) are indicated by red asterisks and red brackets. After PNGase F treatment, the single-chain product shifts to ~250 kDa and the heavy-chain converts into a sharp band at 160-170 kDa, marked by a red triangle. The I22I variant shows two stable bands at ~250 kDa (SC^{mut}, blue asterisk) and 160-170 kDa (HC, blue triangle), both unchanged after PNGase F digestion. The R2228X variant displays a single-chain product above 250 kDa (pale-pink asterisk) and a heavy-chain region between 120 and 200 kDa (pale-pink bracket) that collapses into a distinct band after PNGase F treatment. The R1960X variant is marked with cyan asterisks and cyan triangles, showing faint single- and heavy-chain signals with a broad smear that intensifies after PNGase F treatment.

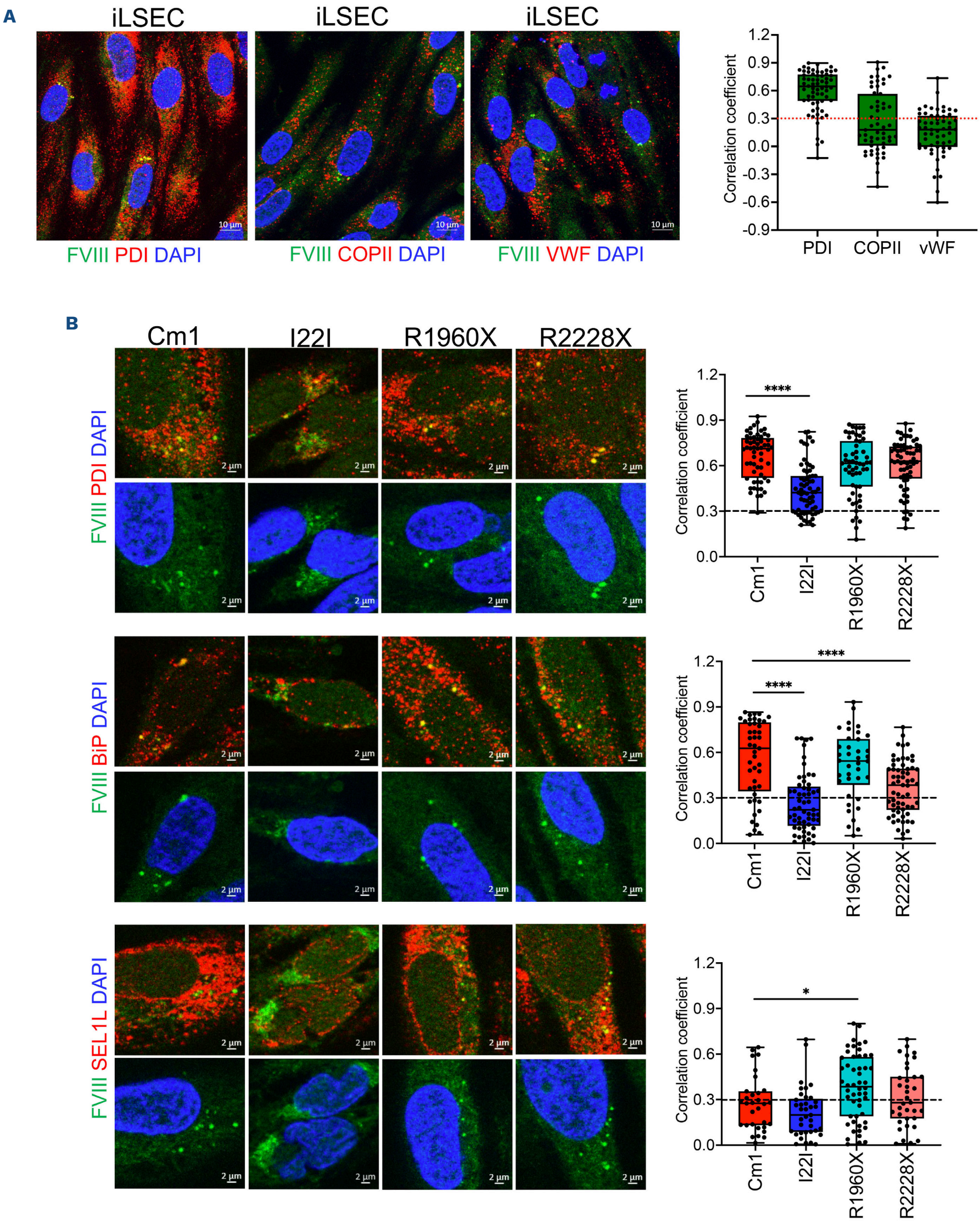

Figure 8. Subcellular localization and endoplasmic reticulum retention of wild-type and mutant FVIII in induced liver sinusoidal endothelial cells. (A) FVIII wild-type (green) is co-localizing with Endoplasmic Reticulum-Marker PDI (red) showing a mean Pearson's correlation coefficient (PCC) of 0.6 (left panel). Minimal co-localization was observed between FVIII and individual COPII

Continued on following page.

vesicles with mean PCC of 0.3 (middle panel). Co-localization between FVIII and von Willebrand factor (VWF) was mostly absent showing mean PCC of 0.1 (left panel). Nuclei were counterstained with DAPi. Results depicted as a representative image of biological triplicates. (B) Comparison of the intracellular localization of wild-type (Cm1) and mutant FVIII (I22I, R1960X, R2228X) variants in induced liver sinusoidal endothelial cells (iLSEC). Co-localization of FVIII (green) was analyzed with PDI (red, top row), BiP (red, middle row), and SEL1L (red, bottom row). The nuclei are counterstained with DAPi (blue). FVIII with PDI (top row) indicates significant ER retention for Cm1, R1960X and R2228X with mean PCC of 0.6 and reduction of co-localization for intron 22 inversions (I22I) with mean PCC of 0.4 in the corresponding boxplot. FVIII with BiP (middle row) demonstrates co-localization for Cm1, R1960X with mean PCC of 0.5, and R2228X with mean PCC of 0.3. Co-localization for I22I and BiP was absent with mean PCC of 0.2. SEL1L (bottom row) presents absence of co-localization with Cm1 or I22I presenting a mean PCC of 0.2. When normalized to wild-type Cm1, both nonsense variants R1960X and R2228X show an increase of co-localization with mean PCC of 0.38 and 0.32. Images were acquired using an Axio Observer 7 microscope with ApoTome.2 with a Plan-Apochromat 40x/1.4 Oil DIC M27 objective. Images were captured with an AxioCam 702 Mono camera. Results depicted as a representative image of biological triplicates. Data are presented as mean ± SEM. Statistical analysis was performed using one-way ANOVA followed by Dunnett's multiple comparison test comparing each variant to the wild-type (Cm1). Significance is indicated as follows: **P*<0.05, ***P*<0.01, ****P*<0.001, *****P*<0.0001." Anova analysis is shown in *Online Supplementary Table S3*.

secretion and no detectable extracellular FVIII activity (*data not shown*). Furthermore, no co-localization of FVIII with von Willebrand Factor (VWF) was observed, suggesting that FVIII and VWF may not be co-synthesized or secreted via shared pathways in this model.

To examine VWF synthesis, we performed VWF immunostaining in the induced models iLSEC and iLEC, as well as in pHUVEC and pHDLEC (*Online Supplementary Figure S12A*). While VWF was detectable in all cell types, only pHDLEC exhibited distinct punctate structures consistent with Weibel-Palade bodies, indicating differential VWF processing in our models. Notably, pHDLEC also showed high *F8* mRNA expression (*Online Supplementary Figure S12B*), but co-staining for FVIII and VWF revealed no co-localization (*Online Supplementary Figure S12C*). This finding contrasts with reports from primary LEC, where FVIII and VWF have been shown to co-localize.[25]

Immunofluorescent staining identifies FVIII variant R1960X in endoplasmic reticulum degradative pathway

We aimed to elucidate the processing of FVIII variants, especially in the context of degradation and immunogenicity. Co-staining experiments were conducted to assess the localization and potential fate of wild-type and variant forms of FVIII (Biotin anti-FVIII conjugate) within the ER. Wild-type (Cm1) and both FVIII variants R1960X & R2228X highly co-localized with PDI with a Pearson´s correlation coefficient (PCC) of 0.6, indicating their presence within the ER (Figure 8B and *Online Supplementary Table S3*). For I22I, a significant reduction in co-localization (PCC = 0.4) was observed. BiP, an ER chaperone, also co-localized with FVIII wild-type and nonsense mutation R1960X (PCC = 0.5) (Figure 8B), and to a lower extent with R2228X (PCC = 0.3), implying an involvement of BiP in the folding and processing of FVIII variants within the ER. Notably, the co-localization was significantly low for the I22I variant (PCC = 0.2). SEL1L, a marker for the ER-associated degradation (ERAD-L) pathway, was found to co-localize with the FVIII variant R1960X (PCC = 0.38) and R2228X (PCC = 0.32), but not with Cm1 or I22I (PCC = 0.2) (Figure 8B). The co-localization of SEL1L with both nonsense variants suggests that the FVIII protein is targeted for proteasomal degradation, although to differing extents, with only R1960X showing statistically significant co-localization compared to wild-type.

In addition to these experimental observations, we performed *in silico* predictions of peptide presentation based on the patients' HLA genotypes (*Online Supplementary Table S4*). These exploratory analyses indicated that R1960X may present a higher number of FVIII-derived peptides via HLA-B (MHC-I) as well as HLA-DRB1 and HLA-DQA1/DQB1 (MHC-II) compared to R2228X (*Online Supplementary Figures S13, S14*).

Discussion

There is a strong correlation between the type of *F8* mutation and consequently the residual amount of intracellular protein from null mutations that influences the risk for inhibitor development.[8] Thus, we asked ourselves whether truncated parts of the endogenous FVIII protein being produced could influence the immunogenicity against replacement therapy in HA patients. To answer this question, since the FVIII protein is synthesized and located within sinusoidal and lymphatic EC,[13,14,26] we established two patient-specific iPS-based EC models, iLEC and iLSEC, capable of producing FVIII.

Differentiation towards iLEC involved treatment of vEC to increase lymphangiogenesis. VEGF-C and angiopoietin are known regulators of lymphatic markers such as *LYVE1, VEGFR3, PROX1* and *PDPN*.[27,28] Although upregulation of *LYVE1* and *VEGFR3* was achieved, we observed from varied to no expression in *PROX1* and *PDPN*. Our optimized model combining VEGF-A, VEGF-C, and IL-3 treatments resulted in a 2.3-fold increase in *F8* expression. We also modulated lymphangiogenesis by the NF-kB pathway, since *PROX1* and *VEGFR3* are downstream targets, by testing the inflammatory cytokines.[29] In this approach, a significant upregulation of *F8* expression was observed only in the presence of IL3, suggesting its unique role in promoting *F8* expression. We also observed an antagonistic effect of TNFα on LYVE1 expression, suggesting *LYVE1* has a role

as a gatekeeper that restricts leukocyte trans-lymphatic migration under non-inflammatory conditions.[30] Treatment with IFNγ led to the upregulation of MHC-II molecules, facilitated by the induction of the CIITA transcription factor.[31] The varied responses to different cytokines highlight the inherent complexity of cytokine signaling in endothelial cells, and underscore the importance of considering multiple pathways and interactions when designing strategies to enhance *F8* expression in an immune-modulatory context.
All patient-specific variants were subsequently analyzed using ELISA in the iLEC model, where the first detectable pattern revealed the presence of not only Cm1 and I22I, but also the two light chain variants R1960X and R2228X.
CD144$^+$ cells are considered more mature and committed to endothelial cell lineages involved in lymphatic vascular formation. Interestingly, there is evidence that LSEC arise from a hematopoietic stem cell source during development.[32] This is likely due to shared developmental pathways between endothelial and hematopoietic lineages during mesodermal differentiation through the hemangioblast, which gives rise to both blood cells and endothelial cells.[32-34] Therefore, differentiation towards iLSEC was established by selection of CD34$^+$ angioblasts upon notch signaling inhibition. In the presence of hypoxia, progenitors were maintained in VEGF-A and TGF-β inhibition which led to a 3.3-fold increase of *F8* expression and upregulation of LSEC-specific markers *STAB2, FCGR2b* and *LYVE1*. The FVIII positive samples initially detected in the iLEC model were confirmed in the iLSEC model, and all subsequent downstream analyses were conducted using the iLSEC model.
Recent single-cell RNA sequencing studies have highlighted the intrinsic heterogeneity of primary LSEC, which show zonation-dependent differences in marker expression and function.[33] For instance, central venous LSEC typically express *STAB2, LYVE1, FCGR2b* and *F8* but lack *VWF*, whereas periportal LSEC express *VWF* and *F8* but show reduced levels of these canonical LSEC markers. Consistent with these findings, qRT-PCR analysis revealed that our primary LSEC expressed *F8* but lacked detectable levels of *STAB2* or *FCGR2b*, suggesting a periportal phenotype (Zone 1), whereas our iPSC-derived LSEC appear to represent a more central venous phenotype (Zone 2/3) with stable *STAB2, LYVE1* and *FCGR2b* expression after two days of LSEC induction (LI-2D E/S) (Figure 5A).
There is evidence that LSEC with high *F8* expression often exhibit low *VWF* expression, suggesting an inverse relationship between these two proteins within specific endothelial subpopulations.[13] In our study, we observed no co-localization of FVIII and VWF in either the iPSC-derived endothelial model (iLSEC) or in primary HDLEC. Specifically, only the pHDLEC displayed mature Weibel-Palade bodies as indicated by the distinct VWF staining pattern. In contrast, VWF localization in the iPSC-derived endothelial cells appeared immature and diffuse, lacking typical storage structures. To our knowledge, little is known about the intracellular co-localization dynamics of FVIII and VWF in liver endothelial cells. A single study reported FVIII localization within Weibel-Palade bodies in primary LEC, but our data do not support this observation.[25] Further research is needed to elucidate whether this spatial separation reflects functional divergence or different maturation stages of endothelial subtypes.
While central tolerance is key to FVIII tolerance,[35] peripheral tolerance may be responsible for the existence of anti-FVIII antibodies in healthy individuals.[36,37] Peripheral *F8* expression by non-hematopoietic antigen presenting cells (nhAPC) like LEC and LSEC might be crucial in mediating tolerance to FVIII through immune-modulatory mechanisms such as T-cell deletion, anergy, or induction of regulatory T cells via TGF-β and Notch signaling. LEC present self-proteins via MHC-I in an AIRE-independent manner and promoting tolerance by PD1/PD-L1.[38] Presentation of self-proteins by MHC-II was only reported after transfer to dendritic cells.[39] Similarly, LSEC can engage CD8$^+$ T cells via endogenous antigen presentation.[40,41]
In nhAPC, MHC-I presents peptides generated by the ubiquitin-proteasome system (UPS).[42] During ER-associated degradation (ERAD), misfolded polypeptides are transported out of the ER lumen to be processed by the UPS. The resulting peptides are then transferred back to the ER and loaded onto TAP for presentation by MHC-I.[43] The ERAD-L pathway degrades luminal, aberrantly glycosylated proteins like FVIII.[44] SEL1L is a large ER-luminal receptor that recognizes misfolded substrates via BiP and regulates the ER transmembrane ubiquitin ligase HRD1/gp78, which mediates the first interaction with the UPS during ERAD-L.[45,46]
We also performed *in silico* predictions of peptide presentation based on the HLA genotypes of the 3 protein-positive patients. These exploratory analyses indicated that patient R1960X, who developed an inhibitor, may present a higher number of FVIII-derived peptides via HLA-B (MHC-I) as well as HLA-DRB1 and HLA-DQA1/DQB1 (MHC-II) compared to patients R2228X or I22I. Furthermore, R1960X displayed a DRB1 repertoire enriched for B-domain peptides, whereas such peptides were not predicted for R2228X and I22I. This observation does not contradict our model in which increased proteasomal degradation of truncated FVIII in R1960X could enhance the supply of peptides for MHC presentation, as suggested by the extensive smear pattern in western blot analyses. At the same time, it must be emphasized that these findings are exploratory; binding and processing predictions reflect algorithmic estimates and inherent database biases, and do not demonstrate actual surface presentation or immunogenicity *in vivo* (*Online Supplementary Figures S13, S14*).
Immunofluorescence revealed co-localization of FVIII variant R1960X with SEL1L and BiP demonstrating proteasomal degradation via the ERAD-L pathway. For this patient (R1960X), two immunomodulatory mechanisms may be considered. 1) Under normal physiological conditions, FVIII is presented by MHC-I to CD8$^+$ T cells. Regulatory CD8$^+$

T cells ($CD8^+CD25^+FoxP3^+$) modulate immune responses by directly suppressing $CD4^+$ effector T cells in a MHC-class Ib (Qa-1 in mice and HLA-E in humans) dependent pathway.[47-49] Conversely, the truncated FVIII variant might present an altered peptide pattern disrupting the suppressive environment. 2) Unfolded protein response (UPR) is triggered compromising the tolerogenic functions of LEC and LSEC, shifting their cytokine secretion profiles toward inflammation.[50]

The nonsense variant R2228X localized to the ER and exhibited moderate co-localization with both SEL1L and BiP, suggesting partial involvement of the ERAD-L pathway. Additionally, the western blot pattern of R2228X resembled that of the wild-type protein more closely than R1960X, implying a potential for partial secretion. Notably, the patient harboring the R2228X variant did not develop an inhibitor, raising the question of whether residual secretion or limited degradation of the variant protein might contribute to immune tolerance.

In contrast, the I22I variant co-localized with the ER marker PDI, but showed no significant co-localization with SEL1L or BiP, indicating its retention within the ER without effective engagement of the ERAD-L pathway or proteasomal degradation. This suggests that the truncated protein does not efficiently engage classical quality control mechanisms within the ER. The truncated product might be sequestered in a non-functional, aggregated form, which could lead to ER crowding.

In future investigations, it will be crucial to understand specific MHC-I peptide patterns and cytokine secretion profiles associated with wild-type *versus* FVIII variants. The nonsense mutation patient-specific model enables us to explore PTC, apart from its surrounding sequence-context. It would be interesting to determine read-through response in combination with patient-specific NMD machinery and explore the differences in degradation mechanisms of the mutated *F8* transcript among HA patients. Additionally, it remains to be clarified whether the chronic ER retention of I22I-derived truncated FVIII contributes to cellular stress, immune activation or tolerance induction.

This study has some limitations. Detection of the FVIII protein, especially in its functional secreted form, has been challenging. While our attempt to detect intracellular FVIII protein was successful, the secretory pathways might not be fully represented *in vitro*. Finally, while patient-derived iPS cells are extremely valuable, we cannot generalize the findings of this study across all HA patients and genotypes because of individual genetic and epigenetic variability.

In conclusion, we established a patient-specific HA cellular model for the endogenous detection of FVIII. By this we detected and localized for the first time endogenous FVIII light chain PTC variants R1960X and R2228X. Additionally, we confirmed the existence of an I22I-derived FVIII variant. Our findings suggest that the differential processing and intracellular localization of FVIII variants, particularly the interaction with the ERAD-L pathway, may contribute to the hierarchical risk of inhibitor formation. This underscores the need for further investigation into patient-specific FVIII variants and their immunogenic potential, especially in relation to antigen presentation and regulatory T-cell function.

Disclosures

No conflicts of interest to disclose.

Contributions

HS and JO are responsible for the study concept; FF, KJC and HS are responsible for the development of F8-/-; HS and RA are responsible for the establishment of vEC; HS and PC are responsible for the establishment of iLEC and iLSEC; HS, PC and TF are responsible for the analysis and interpretation of data cell culture, RT-qPCR, and western blot; PC, MS and HS are responsible for the analysis and interpretation of MassSpec data; HS and PE are responsible for the data cytokine influence; PC and JM are responsible for the FACS analysis; MR gave technical support; BP carried out HLA genotyping; HS and PC are responsible for in silico peptide binding prediction; HS and PC wrote the original draft; PC, OEM and BP wrote, reviewed and edited the manuscript; HS and JO supervised the study.

Acknowledgments

Primary liver sinusoidal endothelial cells were a kind gift from Dr. Osman El-Maarri. FVIII reference peptide library was created using a plasma-derived FVIII product and the experiment was conducted by Dr. Samhitha Urs and Dr. Arijit Biswas. Protein identification was performed at the Core Facility Analytical Proteomics, Institute of Biochemistry and Molecular Biology, Medical Faculty, University of Bonn. We also thank the Bonn Haemophilia Centre, in particular Dr. C. Klein and Dr. K. Herbst, for their support in collecting patient blood samples.

Funding

This work was supported, in part, by funding from Bayer Vital #KEL056 (to JO/OEM/HS), ECIA 2017 from Bayer (to HS), Horizon 2020 Marie Curie ITN EDUC8 grant #859974 (to PC), DFG Emmy Noether Programme #CZ-245 (to KJCN), and a scientific grant from Octapharma #OCT-23-002 (to JO/HS). Protein identification was funded by the Deutsche Forschungsgemeinschaft (DFG, German Research Foundation) – Project number 386936527.

Data-sharing statement

The original western blot images and microscopy data reported in this paper will be shared on request by the corresponding author, Prof. Dr. med. Johannes Oldenburg (johannes.oldenburg@ukbonn.de). Any additional information required to reanalyze the data reported in this paper, and any requests for resources and reagents should be directed to and will be fulfilled by Prof. Oldenburg.

References

1. Franchini M, Mannucci PM. Past, present and future of hemophilia: a narrative review. Orphanet J Rare Dis. 2012;7:24.
2. Garagiola I, Palla R, Peyvandi F. Risk factors for inhibitor development in severe hemophilia a. Thromb Res. 2018;168:20-27.
3. Oldenburg J, Pavlova A. Genetic risk factors for inhibitors to factors VIII and IX. Haemophilia. 2006;12(6):15-22.
4. Astermark J, Oldenburg J, Carlson J, et al. Polymorphisms in the TNFA gene and the risk of inhibitor development in patients with hemophilia A. Blood. 2006;108(12):3739-3745.
5. Astermark J, Oldenburg J, Pavlova A, Berntorp E, Lefvert AK, Group MS. Polymorphisms in the IL10 but not in the IL1beta and IL4 genes are associated with inhibitor development in patients with hemophilia A. Blood. 2006;107(8):3167-3172.
6. Astermark J, Wang X, Oldenburg J, Berntorp E, Lefvert AK, Group MS. Polymorphisms in the CTLA-4 gene and inhibitor development in patients with severe hemophilia A. J Thromb Haemost. 2007;5(2):263-265.
7. David D, Santos IM, Johnson K, Tuddenham EGD, McVey JH. Analysis of the consequences of premature termination codons within factor VIII coding sequences. J Thromb Haemost. 2003;1(1):139-146.
8. Gouw SC, van den Berg HM, Oldenburg J, et al. F8 gene mutation type and inhibitor development in patients with severe hemophilia A: systematic review and meta-analysis. Blood. 2012;119(12):2922-2934.
9. Testa MF, Lombardi S, Bernardi F, et al. Translational readthrough at F8 nonsense variants in the factor VIII B domain contributes to residual expression and lowers inhibitor association. Haematologica. 2023;108(2):472-482.
10. Pandey GS, Yanover C, Miller-Jenkins LM, et al. Endogenous factor VIII synthesis from the intron 22-inverted F8 locus may modulate the immunogenicity of replacement therapy for hemophilia A. Nat Med. 2013;19(10):1318-1324.
11. Vir P, Gunasekera D, Dorjbal B, et al. Lack of factor VIII detection in humans and dogs with an intron 22 inversion challenges hypothesis regarding inhibitor risk. J Thromb Haemost. 2024;22(12):3415-3430.
12. Bernabeu-Herrero ME, Patel D, Bielowka A, et al. Mutations causing premature termination codons discriminate and generate cellular and clinical variability in HHT. Blood. 2024;143(22):2314-2331.
13. Pan J, Dinh TT, Rajaraman A, et al. Patterns of expression of factor VIII and von Willebrand factor by endothelial cell subsets in vivo. Blood. 2016;128(1):104-109.
14. Jacquemin M, Neyrinck A, Hermanns MI, et al. FVIII production by human lung microvascular endothelial cells. Blood. 2006;108(2):515-517.
15. Shahani T, Lavend'homme R, Luttun A, Saint-Remy JM, Peerlinck K, Jacquemin M. Activation of human endothelial cells from specific vascular beds induces the release of a FVIII storage pool. Blood. 2010;115(23):4902-4909.
16. Koch PS, Lee KH, Goerdt S, Augustin HG. Angiodiversity and organotypic functions of sinusoidal endothelial cells. Angiogenesis. 2021;24(2):289-310.
17. Gage BK, Liu JC, Innes BT, et al. Generation of functional liver sinusoidal endothelial cells from human pluripotent stem-cell-derived venous angioblasts. Cell Stem Cell. 2020;27(2):254-269.e259.
18. Koui Y, Kido T, Ito T, et al. An in vitro human liver model by iPSC-derived parenchymal and non-parenchymal cells. Stem Cell Rep. 2017;9(2):490-498.
19. Jamil MA, Singer H, Al-Rifai R, et al. Molecular analysis of fetal and adult primary human liver sinusoidal endothelial cells: a comparison to other endothelial cells. Int J Mol Sci. 2020;21(20):7776.
20. Patsch C, Challet-Meylan L, Thoma EC, et al. Generation of vascular endothelial and smooth muscle cells from human pluripotent stem cells. Nat Cell Biol. 2015;17(8):994-1003.
21. Fahs SA HM, Shi Q, Weiler H, Montgomery RR. A conditional knockout mouse model reveals endothelial cells as the principal and possibly exclusive source of plasma factor VIII. Blood. 2014;123(24):3706-3713.
22. Arai T, Sakurai T, Kamiyoshi A, et al. Induction of LYVE-1/stabilin-2-positive liver sinusoidal endothelial-like cells from embryoid bodies by modulation of adrenomedullin-RAMP2 signaling. Peptides. 2011;32(9):1855-1865.
23. Hen G, Nicenboim J, Mayseless O, et al. Venous-derived angioblasts generate organ-specific vessels during zebrafish embryonic development. Development. 2015;142(24):4266-4278.
24. Zhang H, Pu W, Tian X, et al. Genetic lineage tracing identifies endocardial origin of liver vasculature. Nat Genet. 2016;48(5):537-543.
25. Hough C, Notley C, Mo A, Videl B, Lillicrap D. Heterogeneity and reciprocity of FVIII and VWF expression, and the response to shear stress in cultured human endothelial cells. J Thromb Haemost. 2022;20(11):2507-2518.
26. Shahani T, Covens K, Lavend'homme R, et al. Human liver sinusoidal endothelial cells but not hepatocytes contain FVIII. J Thromb Haemost. 2014;12(1):36-42.
27. Lee SJ, Park C, Lee JY, et al. Generation of pure lymphatic endothelial cells from human pluripotent stem cells and their therapeutic effects on wound repair. Sci Rep. 2015;5:11019.
28. Rufaihah AJ, Huang NF, Kim J, et al. Human induced pluripotent stem cell-derived endothelial cells exhibit functional heterogeneity. Am J Transl Res. 2013;5(1):21-35.
29. Flister MJ, Wilber A, Hall KL, et al. Inflammation induces lymphangiogenesis through up-regulation of VEGFR-3 mediated by NF-kappaB and Prox1. Blood. 2010;115(2):418-429.
30. Johnson LA, Prevo R, Clasper S, Jackson DG. Inflammation-induced uptake and degradation of the lymphatic endothelial hyaluronan receptor LYVE-1. J Biol Chem. 2007;282(46):33671-33680.
31. Steimle V, Siegrist CA, Mottet A, Lisowska-Grospierre B, Mach B. Regulation of MHC class II expression by interferon-gamma mediated by the transactivator gene CIITA. Science. 1994;265(5168):106-109.
32. Ditadi A, Sturgeon CM. Directed differentiation of definitive hemogenic endothelium and hematopoietic progenitors from human pluripotent stem cells. Methods. 2016;101:65-72.
33. MacParland SA, Liu JC, Ma XZ, et al. Single cell RNA sequencing of human liver reveals distinct intrahepatic macrophage populations. Nat Commun. 2018;9(1):4383.
34. Scarfo R, Randolph LN, Abou Alezz M, et al. CD32 captures committed haemogenic endothelial cells during human embryonic development. Nat Cell Biol. 2024;26(5):719-730.
35. Madoiwa S, Yamauchi T, Kobayashi E, et al. Induction of factor VIII-specific unresponsiveness by intrathymic factor VIII injection in murine hemophilia A. J Thromb Haemost. 2009;7(5):811-824.
36. Meunier S, Menier C, Marcon E, Lacroix-Desmazes S, Maillere B. CD4 T cells specific for factor VIII are present at high frequency

in healthy donors and comprise naive and memory cells. Blood Adv. 2017;1(21):1842-1847.
37. Porcheddu V, Lhomme G, Giraudet R, Correia E, Maillere B. The self-reactive FVIII T cell repertoire in healthy individuals relies on a short set of epitopes and public clonotypes. Front Immunol. 2024;15:1345195.
38. Rouhani SJ, Eccles JD, Tewalt EF, Engelhard VH. Regulation of T-cell tolerance by lymphatic endothelial cells. J Clin Cell Immunol. 2014;5:1000242.
39. Dubrot J, Duraes FV, Potin L, et al. Lymph node stromal cells acquire peptide-MHCII complexes from dendritic cells and induce antigen-specific CD4(+) T cell tolerance. J Exp Med. 2014;211(6):1153-1166.
40. Knolle PA, Wohlleber D. Immunological functions of liver sinusoidal endothelial cells. Cell Mol Immunol. 2016;13(3):347-353.
41. Xu X, Jin R, Li M, et al. Liver sinusoidal endothelial cells induce tolerance of autoreactive CD4+ recent thymic emigrants. Sci Rep. 2016;6:19861.
42. ten Broeke T, Wubbolts R, Stoorvogel W. MHC class II antigen presentation by dendritic cells regulated through endosomal sorting. Cold Spring Harb Perspect Biol. 2013;5(12):a016873.
43. Blum JS, Wearsch PA, Cresswell P. Pathways of antigen processing. Annu Rev Immunol. 2013;31:443-473.
44. Berner N, Reutter KR, Wolf DH. Protein quality control of the endoplasmic reticulum and ubiquitin-proteasome-triggered degradation of aberrant proteins: yeast pioneers the path. Annu Rev Biochem. 2018;87:751-782.
45. Christianson JC, Ye Y. Cleaning up in the endoplasmic reticulum: ubiquitin in charge. Nat Struct Mol Biol. 2014;21(4):325-335.
46. Mueller B, Lilley BN, Ploegh HL. SEL1L, the homologue of yeast Hrd3p, is involved in protein dislocation from the mammalian ER. J Cell Biol. 2006;175(2):261-270.
47. Wang YM, Alexander SI. CD8 regulatory T cells: what's old is now new. Immunol Cell Biol. 2009;87(3):192-193.
48. Jiang H, Wu Y, Liang B, et al. An affinity/avidity model of peripheral T cell regulation. J Clin Invest. 2005;115(2):302-312.
49. Jiang H, Chess L. The specific regulation of immune responses by CD8+ T cells restricted by the MHC class Ib molecule, Qa-1. Annu Rev Immunol. 2000;18:185-216.
50. So JS. Roles of endoplasmic reticulum stress in immune responses. Mol Cells. 2018;41(8):705-716.